PCCP

# Adsorption of $CS_2$ on MgO microcrystals: formation of a S-doped MgO surface

**Domenica Scarano,[a] Serena Bertarione,[a] Adriano Zecchina,[a] Raffaella Soave[b] and Gianfranco Pacchioni[b]**

[a] *Dipartimento di Chimica Inorganica, Chimica Fisica e Chimica dei Materiali, Università di Torino, Via P. Giuria 7, 10125 Torino, Italy*
[b] *Dipartimento di Scienza dei Materiali, Università di Milano-Bicocca, Istituto Nazionale per la Fisica della Materia, Via R. Cozzi, 53, 20125 Milano, Italy*

***Received 23rd May 2001, Accepted 25th October 2001***
***First published as an Advance Article on the web***



The interaction of carbon disulfide, $CS_2$, with polycrystalline MgO was investigated by means of infrared and UV–visible spectroscopies and *ab initio* electronic structure calculations. The aim was to understand the modifications of the surface properties of MgO microcrystals induced by the substitution of $O^{2-}$ with $S^{2-}$ anions. The interaction of $CS_2$ with MgO shows the formation of thiocarbonates followed by O–S exchange reactions and formation of $Mg^{2+}$–$S^{2-}$ clusters in a MgO matrix. The O–S exchange reaction involves mainly the low-coordinated $O^{2-}$ anions at the steps and corner sites, and only at high temperature are a small number of $O^{2-}$ anions at the (100) terrace sites involved. The replacement of the O with the S atoms at the low-coordinated sites of the MgO surface transforms the reactive polycrystalline material into a chemically inert system.

## 1. Introduction

High surface area metal oxides exhibit a highly disordered morphology, since the microcrystals are terminated by many crystallographic planes, having a relevant concentration of steps, kinks, edges and other defects, responsible for their high reactivity.[1,2] The investigation of the structure of these highly reactive surfaces, characterized by the presence of coordinatively unsaturated ions, has been the subject of extensive discussion. In particular, in addition to the interaction of simple probe molecules with surface cations,[3–7] the formation of complex anionic species upon interaction of CO, NO, $CO_2$, *etc.* with anionic centers ($O^{2-}$) has been described by several authors.[8–11] On polycrystalline MgO the interaction of CO with surface $O^{2-}$ species, probably located at defect sites, consists in a nucleophilic attack of $O^{2-}$ on adsorbed CO, leading to the formation of multidentate and bidentate $CO_2^{2-}$ species and of ketenic-like dimeric (KD) $C_2O_2^{2-}$ species.[8,12,13] The reactions occur even at low temperatures. This high reactivity contrasts with the total absence of chemical activity of the MgO(100) single crystal face;[14–16] in this case CO adsorbs very weakly on the surface cations with a dissociation energy, $D_e$, of 0.14 eV and desorbs at temperatures above 57 K.[17] This provides indirect but compelling evidence for the important role of the surface defects in the chemistry of MgO.

The aim of this paper was to understand the modifications of the surface properties of MgO microcrystals as a consequence of the replacement of $O^{2-}$ with $S^{2-}$ anions on the surface, this being the first time that S-doped MgO surfaces have been described. The interaction of carbon disulfide, $CS_2$, with polycrystalline MgO shows the occurrence of exchange reactions and formation of $Mg^{2+}$–$S^{2-}$ clusters in the MgO matrix. The presence of the S atoms at the surface of MgO completely changes the reactivity of the oxide, and transforms the reactive polycrystalline material into a chemically inert system. The mechanisms of the interaction of $CS_2$ with various MgO sites, the O–S exchange reaction, and the decoration of the surface by S atoms have been investigated by means of IR and UV spectroscopies and first principle theoretical calculations. The formation of $Mg^{2+}$–$S^{2-}$ clusters in the MgO matrix could represent a simple model for more complex structures such as enzymes, where it is known that metal–sulfur fragments are the active sites in many enzyme-catalyzed reactions. In particular, it was reported that some proteins contain crystallographically defined cubane-type clusters, with $Fe_4S_4$ reactive cores, which catalyze metabolic reactions. Such a structure can be well mimicked by defective surfaces of inorganic oxides containing edges and steps decorated by S anions.[18] Furthermore, the interaction of sulfur-containing molecules with oxide surfaces is relevant for processes involving poisoning and desulfurization reactions.[19]

## 2. Methods

### 2.1 Experimental details

High surface area MgO was prepared by thermal decomposition of brucite, $Mg(OH)_2$, at 520–550 K in vacuum, followed by outgassing in vacuum at 1073 K. The final surface area is about 200 $m^2\ g^{-1}$.

The high surface area MgO samples, obtained as described above, were first dosed with CO at 100 K to check the IR spectra of the species formed upon interaction with CO. After this experiment the sample was outgassed in vacuum at 1073 K to clean the surface of the adsorbed CO, and then dosed with $CS_2$ at 298 K. After $CS_2$ contact at 298 K, the MgO samples were outgassed at 673–773 K, in order to remove the physisorbed carbon disulfide species. Successive re-exposure to CO at 100 K of such sulfide-doped samples gives information on the state of the surface after $CS_2$ contact. The IR spectra were recorded at 2 $cm^{-1}$ resolution on a Bruker IFS48 FTIR spectrometer equipped with an MCT cryogenic detector. Diffuse reflectance UV–visible spectra were also recorded on pure

 DOI: 10.1039/b104566k

and sulfide-doped samples, by means of a Varian Cary 5 spectrometer.

### 2.2 Computational details

The interaction of $CS_2$ with low-coordinated O sites on the MgO surface was studied with cluster models. This method has been widely used to study the adsorption and reaction of molecules with oxide surfaces and it properly describes the physics of local surface processes.[20,21] Owing to the highly ionic nature of MgO, the truncation of the crystal lattice implies the use of an external field to represent the long-range Coulomb potential. All the selected model clusters were embedded in a large array of point charges, PC, set to the nominal value $\pm 2$ in order to reproduce the correct Madelung potential at the adsorption site.[22] Previous studies[23–25] have demonstrated that the use of PCs for embedding can significantly affect the calculated adsorption properties when the positive PCs are nearest neighbors to the highly polarizable oxygen anions of the clusters. In this case, an artificial polarization of the oxygen anions at the cluster borders results; however, this artifact can be eliminated by using an effective core potential (ECP) instead of positive PCs.[26,27] The clusters used to describe the different sites on the MgO surface are (Fig. 1): (a) $[O_{13}Mg_{13}] + ECP_{16} + PCs$ for the $O_{5c}^{2-}$ anion at a terrace site; (b) $[O_{15}Mg_{11}] + ECP_{25} + PCs$ for the $O_{4c}^{2-}$ anion at a stepped surface; (c) $[O_{10}Mg_{10}] + ECP_{10} + PCs$ for the $O_{4c}^{2-}$ anion at an edge site; (d) $[O_{13}Mg_{13}] + ECP_{12} + PCs$ for the $O_{3c}^{2-}$ anion at a corner site. In all the systems, ions, ECPs and PCs taken together give an electrically neutral system.

The calculations were performed with the gradient-corrected density functional theory (DFT) method. We have used Becke's three parameters hybrid exchange functional[28] in combination with the correlation functional of Lee, Yang and Parr[29] (B3LYP). Gaussian-type atomic orbital basis sets were used to construct the Kohn–Sham orbitals. The basis set adopted for the $CS_2$ and COS molecules, the $O^{2-}/S^{2-}$ active anions and the nearest $Mg^{2+}$ neighbor ions was 6-31G*.[30] Some tests using the more complete 6-31 + G* basis set for the admolecules were performed, but the results did not change significantly. For the next nearest neighbor $O^{2-}$ anions we have adopted the 6-31G basis set, while for all the remaining ions we used the 3-21G basis.[31]

The geometry of adsorbed $CS_2$ was fully optimized by means of analytical gradients. In the MgO clusters the O and Mg ion nearest neighbors to the adsorbing O site (if not directly in contact with point charges) were free to move, while the positions of all the other Mg atoms were kept fixed at bulk values. All the binding energies, $D_e$, were corrected by the basis set superposition error (BSSE) by applying the standard counterpoise method.[32]

A full vibrational analysis, based on second derivatives of the total energy, was performed to compute the harmonic frequencies of $CS_2$ adsorbed on the various sites of MgO. The geometries of the transition states, identified by means of a vibrational analysis, of the reaction $MgO + CS_2 \rightarrow MgO(S) + COS$ were determined using the Berny algorithm.[33,34] The calculations were performed with the GAUSSIAN98 program package.

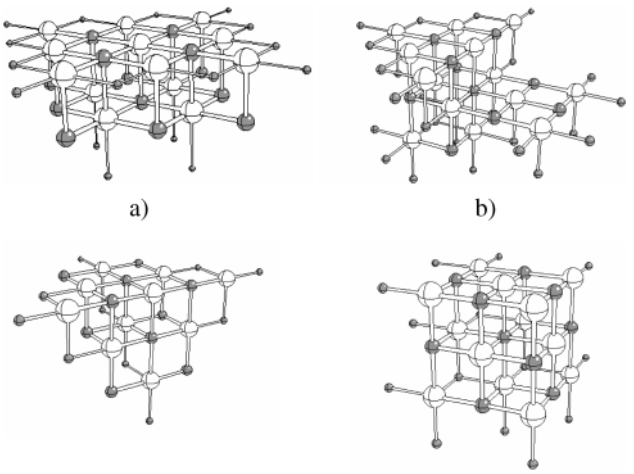


**Fig. 1** Cluster models adopted for the study of $CS_2$ adsorbed on different O sites of MgO. (a) $O_{13}Mg_{13}ECP_{16}$, terrace $O_{5c}^{2-}$; (b) $O_{15}Mg_{11}ECP_{25}$, step $O_{4c}^{2-}$; (c) $O_{10}Mg_{10}ECP_{10}$, edge $O_{4c}^{2-}$; (d) $O_{13}Mg_{13}ECP_{12}$, corner $O_{3c}^{2-}$. White spheres: O atoms, gray spheres: Mg atoms; small gray spheres: ECPs. The clusters are embedded in a large array of PCs (not shown).

## 3. Spectra and reactivity

### 3.1 The morphology of MgO samples

In this process the hexagonal platelets of brucite are topotactically transformed into aggregated cubelets, as shown by transmission electron micrographs, Fig. 2.[14] In these cubelets the presence of different regions can be clearly distinguished; in particular one can see extended, almost flat and scarcely defective zones and stepped terraces. The interference fringes, about 2.07 Å apart, are originating from (400) crystallographic planes; their orientation with respect to the traces of the borders of the microcrystals allows one to conclude that the (100) planes are preferentially exposed.

Different kinds of coordinatively unsaturated $Mg^{2+}$ and $O^{2-}$ ions are present on the surface: 5-fold coordinated $Mg_{5c}^{2+}$ and $O_{5c}^{2-}$ on the extended (100) terraces and faces; 4-fold coordinated $Mg_{4c}^{2+}$ and $O_{4c}^{2-}$ on the edges and steps; 3-fold coordinated $Mg_{3c}^{2+}$ and $O_{3c}^{2-}$ on the corners.

### 3.2 Interaction of CO with pure MgO samples

Exposure of pure MgO samples to CO gives a very complex IR spectrum, which has been the subject of many detailed investigations.[3,4] Polycrystalline MgO reacts with CO at 100 K with initial formation of $CO_2^{2-}$ species (T doublet at 1325 and 1285 $cm^{-1}$ in the IR spectra, Fig. 3), generated by nucleophilic attack of a surface $O^{2-}$ anion on CO weakly bound on a $Mg^{2+}$ cation in an adjacent position. By CO addition at 100 K, the $CO_2^{2-}$ multidentate species are transformed into T′ species characterized by a single peak at 1475 $cm^{-1}$, which is indicative of the presence of an uncoupled CO mode. At the same time, a

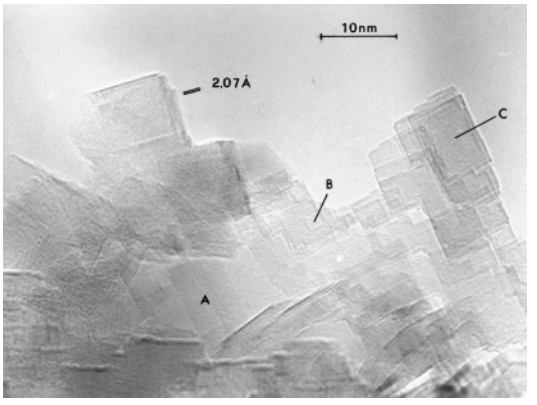


**Fig. 2** High resolution transmission electron micrograph of MgO microcrystals, where different regions can be distinguished. A: extended, almost flat and scarcely defective zones, covering areas of 15–20 × $10^3$ $Å^2$; B and C: stepped terraces with dimensions of 350 and 7500 $Å^2$, respectively.

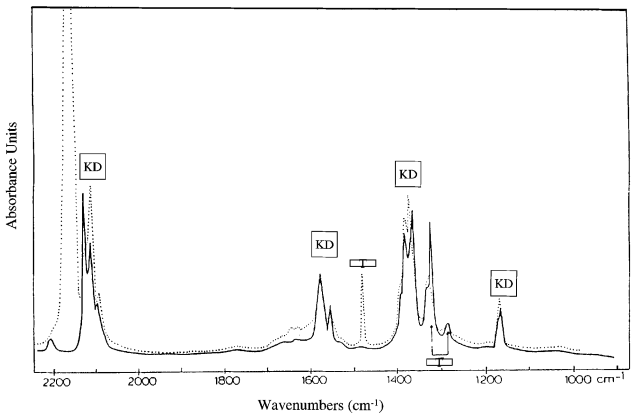


**Fig. 3** FTIR spectra of CO adsorbed at 100 K on MgO at increasing coverages, (continuous line: $p_{CO} = 133$ Pa, dotted line: $p_{CO} = 532$ Pa). KD is related to ketenic-like dimeric $C_2O_2^{2-}$ species; T and T′ are associated with multidentate (T) and bidentate (T′) $CO_2^{2-}$ transient species, which by CO addition, lead to KD species.

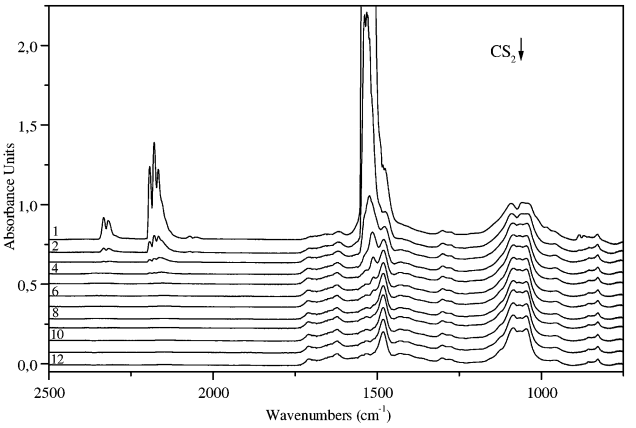


**Fig. 4** FTIR spectra of $CS_2$ adsorbed at 298 K on MgO. The experiment was performed as follows: the sample was first equilibrated with 2.66 kPa pressure of $CS_2$ at RT (spectrum 1); then the pressure was gradually reduced to 0.133 Pa (spectra 2–12).

strong absorption centered at 2160–2150 $cm^{-1}$ develops, which is associated with the stretching mode of CO species bonded or polarized by $Mg^{2+}$ ions. By increasing the CO pressure the T′ species are transformed into dimeric KD species (couples of bands in the 2108–2084 and 1392–1358 $cm^{-1}$ regions, assigned to the antisymmetric and symmetric modes of a first family of ketenic-like dimeric $C_2O_2^{2-}$ species, together with pairs of bands in the 1582–1548 and 1160 $cm^{-1}$ regions associated with a second family of $C_2O_2^{2-}$ dimers). The whole sequence occurring at 100 K, where the last compound ($C_3O_4^{2-}$ trimer) well explains the bands characteristic of the KD species, has been described in detail in a previous paper.[8]

As far as the present study is concerned, we recall that all the previously discussed species are formed by CO attack on the highly reactive and coordinatively unsaturated $O^{2-}$ anions located on edges and corners, which play a key role in determining the formation of negatively charged $C_nO_{n+1}^{2-}$ species.[8,9] The formation of these anionic products is a direct consequence of the high basicity of the $O_{3c,4c}^{2-}$ species.[11] In contrast, it was demonstrated that coordinatively unsaturated $O^{2-}$ and $Mg^{2+}$ ions exposed on extended faces are not reactive towards CO.[9,17]

### 3.3 Interaction of $CS_2$ with pure MgO samples

**3.3.1 Infrared spectra.** The intense and complex IR band, observed at 1525 $cm^{-1}$, is ascribed to a $CS_2$ physisorbed species, because it is reversible by outgassing at 293 K (Fig. 4). [Notice that $CS_2$ in the gas phase exhibits $\nu(CS_2)$ at 1533 $cm^{-1}$ and that metal σ-bonded structures are reported at 1510 $cm^{-1}$.[35] Lavalley *et al.*[36] found a similar band at 1516–1567 $cm^{-1}$ for $CS_2$ on γ-$Al_2O_3$, ZnO and $CeO_2$].

Four-fold and three-fold coordinated $O^{2-}$ ions, located on edges and corners, can react with $CS_2$ in a way similar to that found for $CO_2$,[37] following the paths shown in reactions (1) and (2):

$$O_{4c}^{2-}Mg^{2+}O_{3c}^{2-}O_{4c}^{2-} + CS_2 \rightarrow O_{4c}^{2-}Mg^{2+}[OCS_2]^{2-}O_{4c}^{2-} \rightarrow S_{4c}^{2-}Mg^{2+}[OCOS]^{2-}O_{4c}^{2-} \rightarrow S_{4c}^{2-}Mg^{2+}[OCO_2]^{2-}S_{4c}^{2-} \quad (1)$$

Reaction (1) occurs supposedly at the corners (because the $O_{3c}^{2-}$ ions have three $O_{4c}^{2-}$ ions in adjacent positions), while reaction (2) involves more O anions at steps and edges:

$$O^{2-}{}_{4c}Mg^{2+}O^{2-}{}_{4c} + CS_2 \rightarrow O^{2-}{}_{4c}Mg^{2+}[OCS_2]^{2-} \rightarrow S^{2-}{}_{4c}Mg^{2+}[OCOS]^{2-} \quad (2)$$

The $[OCS_2]^{2-}$, $[OCOS]^{2-}$, and $[OCO_2]^{2-}$ species formed according to reaction (1) can have multidentate character, as shown in Scheme 1 for the $[OCS_2]^{2-}$ structure.

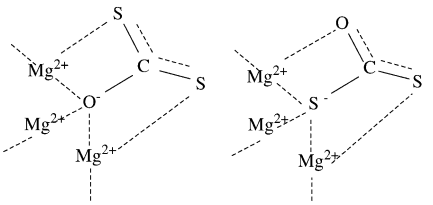


**Scheme 1**

The structures formed following reaction (2) (involving step sites) could be in a form similar to that observed for $CO_2$ adsorbed in the so called organic carbonates (Scheme 2).

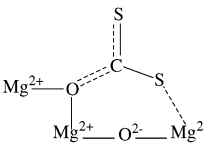


**Scheme 2**

Upon decreasing the equilibrium pressure of $CS_2$, the absorptions centered at ~2350 (weak), 2180 (weak), 2065 (very weak), 1525 (very strong) and 850 $cm^{-1}$ disappear. The absorptions at ~2350, 2180 and 2065 $cm^{-1}$ (with the characteristic rotovibrational envelopes) are due to $CO_2$ (2350 $cm^{-1}$, $\nu_{as}$), $CS_2$ (combination mode: $\nu_1 + \nu_3 = 2180$ $cm^{-1}$) and COS (2065 and 850 $cm^{-1}$) respectively. The shape of the absorption centered at 1525 $cm^{-1}$ ($\nu_{as}$ of $CS_2$) on spectrum 1 of Fig. 4 cannot be singled out, because of its intensity.

This attribution finds support from the infrared photoacoustic spectroscopy (PAS) data of xanthate adsorbed on minerals, where the minor components observed at 2350 and 2065 $cm^{-1}$ have been assigned to $CO_2$ and COS gas-phase species, respectively [see ref. 38 and ref. 8 and 9 cited therein]. It is noteworthy that the presence of bands due to a small amount of $CO_2$ and COS in the gas phase indicates that, after equilibration at room temperature (RT), the exchange reactions have taken place through the formation of $[OCS_2]^{2-}$ and $[OCOS]^{2-}$ intermediates:

$$O_{surf}{}^{2-} + CS_2 \rightarrow [OCS_2]_{ads}{}^{2-} \rightarrow COS + S_{surf}{}^{2-} \quad (3)$$

$$COS + O_{surf}{}^{2-} \rightarrow [OCOS]_{ads}{}^{2-} \rightarrow CO_2 + S_{surf}{}^{2-} \quad (4)$$

As $CO_2$ is observed in the gas phase, the presence of surface carbonates $[CO_3]^{2-}$ cannot be excluded. This behavior is similar to that found by Lavalley *et al.* on $CeO_2$.[36]

After prolonged outgassing at RT (spectrum 12 in Fig. 4), many bands due to irreversibly adsorbed species can be observed at: 1750–1600 (weak doublet); 1550 (weak); 1480 (medium); 1420–1400 (weak doublet); 1350–1250 (weak doublet); 1100 (weak shoulder); 1125–1025 (medium triplet); 950 (weak); and 800–780 $cm^{-1}$ (doublet). This great variety of bands can be explained only on the basis of a plurality of adsorbed structures of the $[OCS_2]^{2-}$, $[OCOS]^{2-}$ and $[CO_3]^{2-}$ type. Moreover their medium–low intensity indicates that these species are not formed on the extended (100) facelets and terraces, which represent 98% of the total surface area.

In order to assign the peaks belonging to the sulfur-containing species, we have to assign first the peaks belonging to $[CO_3]^{2-}$ species, which are better known. Comparison with the results obtained on pure MgO[37] indicates, beyond any doubt, that the peaks at 1750–1600, 1350–1250, 1550 and 1420–1400 $cm^{-1}$ belong to bidentate and monodentate carbonate species, respectively. The doublet at 800–780 $cm^{-1}$ is also ascribed to $[CO_3]^{2-}$ species. After this attribution one can conclude that the features at 1480 and 1125–1025 $cm^{-1}$ can be attributed to $[CS_2O]^{2-}$ and $[CO_2S]^{2-}$ species.

It is difficult to proceed further in the attribution, since depending on the monodentate or bidentate structures, both species can have bands in the two above-mentioned regions,[39] as can be deduced by an examination of the relevant literature on $CS_2$ adsorbed on oxides,[36] or on $[OCS_2]^{2-}$ specie in cryogenic matrices.[40,41] We suggest that $[OCS_2]^{2-}$ species are primarily responsible for the 1125–1025 $cm^{-1}$ adsorption ($\nu(CS)_2$ stretching modes of the $[OCS_2]^{2-}$ groups), while the 1480 $cm^{-1}$ peak is nearly associated with $[OCOS]^{2-}$ species. The assignment of the 1125–1025 $cm^{-1}$ band to $\nu(CS)_2$ of the $[OCS_2]^{2-}$ group is supported by the quantum chemical calculations, see Section 4. Fairly conclusive considerations can be obtained by studying the spectra of samples treated with $CS_2$ at different temperatures (which are expected to contain different proportions of $[OCS_2]^{2-}$ and $[OCOS]^{2-}$ species). From preliminary results, it seems that by increasing the temperature both species ($[OCS_2]^{2-}$ and $[OCOS]^{2-}$) decompose following the exchange reactions (1) and (2), but the COS molecules do not react with $O_{surf}{}^{2-}$ to give $[OCOS]^{2-}$ and then $CO_2$ because most of the oxygen surface sites are substituted by sulfur anions. Hence a higher concentration of $[OCS_2]^{2-}$ species can be suggested.

**3.3.2 UV–visible spectra.** Although a clear distinction between the bidentate and unidentate structures for the adsorbed thiocarbonate species cannot be made on the basis of IR data only, it is likely that bidentate structures can be stabilized by interaction with the surface $Mg^{2+}$ cations, as shown in Scheme 1. The formation of $[OCS_2]^{2-}$ and $[OCOS]^2$ intermediate species can be studied by UV–visible spectroscopy, Fig. 5. Upon $CS_2$ adsorption (dashed line) and successive evacuation at RT (dotted line), an intense band at ~31 500 $cm^{-1}$ and a weaker one at ~26 500 $cm^{-1}$ are observed: these bands can be associated in general with two different types of transitions: the first arises from a $\pi \rightarrow \pi^*$ transition (allowed and then very intense). This is typical of a delocalized system, where the double bond can be shared among oxygen, carbon and sulfur atoms as in the carbonate-like structures. The second feature, appearing as a shoulder of the most intense band at longer wavelengths, could be assigned to a $n \rightarrow \pi^*$ transition (very weak as these

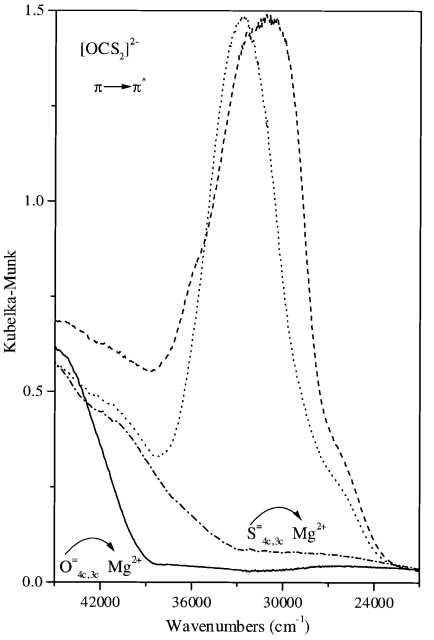


**Fig. 5** UV–visible spectra of $CS_2$ adsorbed at 298 K on MgO ($p_{CS_2}$ = 2.66 kPa). Continuous line: MgO outgassed at 1073 K; dashed line: MgO dosed with $CS_2$ gas; dotted line: MgO dosed with $CS_2$ and outgassed at 298 K; dotted–dashed line: MgO dosed with $CS_2$ and outgassed at 673–773 K.

transitions are generally forbidden) of the C=S chromophore; this is supported by the fact that similar transitions have been observed at 390 nm (~25 600 $cm^{-1}$) in potassium alkyl xanthates.[42]

For a more precise assignment of the bands, the following preliminary considerations on the electronic spectra of $[CO_3]^{2-}$, $[OCOS]^{2-}$, $[OCS_2]^{2-}$ and $[CS_3]^{2-}$ anions must be considered. Let us start from the better known $[CO_3]^{2-}$ anion. For this species two absorption bands are expected, a strong one at ~50 000 $cm^{-1}$ ($\pi \rightarrow \pi^*$)[43] and a much weaker one at ~45 000 $cm^{-1}$ ($n \rightarrow \pi^*$).[42] The $\pi \rightarrow \pi^*$ transition has distinct charge-transfer character. Substitution of oxygen with sulfur to give $[OCOS]^{2-}$, $[OCS_2]^{2-}$ and $[CS_3]^{2-}$ is expected to shift the ($\pi \rightarrow \pi^*$) and ($n \rightarrow \pi^*$) transitions to lower frequencies by a factor of 1.16 $[OCOS]^{2-}$, 1.4 $[OCS_2]^{2-}$ and 1.6 $[CS_3]$[42–44]. Thus, the effect of oxygen–sulfur substitution is to shift the $\pi \rightarrow \pi^*$ transition by a factor of ~1.2. Similar conclusions can be derived by inspection of oxygen–sulfur substitution in CO–CS and $(NH_2)_2CO$–$(NH_2)_2CS$.[44] Following Jörgensen, this corresponds to a modification of the optical electronegativities on passing from oxygen to sulfur ligands,[45] as will be discussed in the following. Similar considerations should also hold for the $n \rightarrow \pi^*$ transitions. Therefore, $[OCS_2]^{2-}$ species are expected to be characterized by a strong $\pi \rightarrow \pi^*$ (charge-transfer) transition at ~36 000 $cm^{-1}$ accompanied by a weaker peak at lower frequency ($n \rightarrow \pi^*$). On this basis the assignment of the strong band at 33 000 $cm^{-1}$ and the shoulder at ~27 500 $cm^{-1}$ in Fig. 5 to $[OCS_2]^{2-}$ is straightforward. It must be recognized however that while the attribution of the main peak to a $\pi \rightarrow \pi^*$ transition is certain, the assignment of the shoulder at ~26 000 $cm^{-1}$ to a $n \rightarrow \pi^*$ transition is debatable. It is possible that it could be ascribed to a $\pi \rightarrow \pi^*$ transition of $[CS_3]^{2-}$ species present in small concentrations. At present, a definitive choice between the two hypotheses cannot be made.

In general a distinction between $\pi \rightarrow \pi^*$ and $n \rightarrow \pi^*$ transitions could be made simply by considering the "solvent effects". As reported in Fig. 5 (dashed line), the main peak undergoes a red-shift in the presence of a multilayer of physically adsorbed $CS_2$. We believe that this is the result of the "solvent effect", even if a correlation with the classical effect

observed in solution must be done with care. In favour of a "solvent effect" we emphasize that the red-shift is totally reversible. In contrast there is no evidence for the shift of the $n \rightarrow \pi^*$ transition, as this latter band merges with the most intense $\pi \rightarrow \pi^*$ band at higher frequency.[42]

A final point that needs to be commented on is related to the erosion of the band, observed on the MgO background at $\sim$44 000 cm$^{-1}$, Fig. 5, caused by $CS_2$ adsorption. This has been assigned to electronic transitions of the excitonic charge-transfer type, an electron being transferred (at least partially) from an oxygen ion to its immediate surroundings.[37,46,47] In particular this excitation can be considered as a charge transfer from $O_{4c}^{2-}$, localized on edge sites, to adjacent $Mg^{2+}$, following the scheme:

$$Mg^{2+}(3s^0)O^{2-}(2p^6) \rightarrow Mg^{2+}(3s^0)O^{2-}(2p^5 3s) \quad (5)$$

$$Mg^{2+}(3s^0)O^{2-}(2p^6) \rightarrow Mg^{+}(3s^1)O^{-}(2p^5) \quad (6)$$

On this basis the observed erosion of the 44 000 cm$^{-1}$ band is a direct consequence of the incorporation of $O^{2-}$ into the $[OCS_2]^{2-}$ species following the scheme:

$$O_{4c}^{2-} + CS_2 \rightarrow [OCS_2]^{2-} \quad (7)$$

After outgassing *in vacuo* in the 673–773 K range (dotted–dashed line), the original spectrum of MgO is not recovered at all and new absorptions (shoulders) are present at $\sim$40 000 and $\sim$36 000 cm$^{-1}$ (while the original band at 44 000 cm$^{-1}$ shows some intensity decrease). We believe that the new bands are associated with a localized excitation:

$$Mg^{2+}S^{2-} \xrightarrow{h\nu} Mg^{+}S^{-} \quad (8)$$

with charge transfer character. A question can now be put forward: is it possible from the spectra of Fig. 5 to gain information on the sites that are preferentially involved in the oxygen–sulfur exchange? To answer this point a digression into the nature of the surface charge transfer (c.t.) bands (excitons) present on alkaline-earth metal oxides is necessary. In particular three absorptions at 53 000, 46 000 and $\sim$37 000 cm$^{-1}$ were found on MgO samples and were attributed to five-, four- and three-fold coordinated oxygen ions.[37] In fact, the lower the coordination of the surface oxide ion, the lower will be the frequency of the surface exciton associated with it,[48] as the Madelung potential is progressively reduced as the coordination decreases.

According to Jörgensen,[45] the frequency of the c.t. bands ($\nu_{ct}$) can be described by the empirical and semiquantitative relation:

$$\nu_{ct} = (30\,000\,\text{cm}^{-1})[\kappa_{opt}(X) - \kappa_{opt}(M)] \quad (9)$$

where X is the anion species, M the metal species and $\kappa_{opt}$ the optical electronegativity. In our case X is $O^{2-}$ or $S^{2-}$ and M is $Mg^{2+}$. When two structurally identical or very similar situations are compared (for instance $O^{2-}$ and $S^{2-}$ on terraces, edges or corners), the frequency shift induced by oxygen–sulfur substitution ($\Delta\nu_{sub}$) can be expressed by the relation:

$$\Delta\nu_{sub} = \nu_{ct}^{S} - \nu_{ct}^{O} = (30000\,\text{cm}^{-1})[\kappa_{opt}(S^{2-}) - \kappa_{opt}(O^{2-})] \quad (10)$$

From inspection of data concerning oxygen- and sulfur-containing ligands,[45] the calculated data from the [$\kappa_{opt}$ ($S^{2-}$) – $\kappa_{opt}$ ($O^{2-}$)] difference can be seen to lie between 0.3 and 0.6; in fact in most cases $\kappa_{opt}$ ($O^{2-}$) is close to 3.2 and $\kappa_{opt}$ ($S^{2-}$) ranges from 2.9 to 2.6. This gives values of $\Delta\nu_{sub}$ in the range of about 9000–18 000 cm$^{-1}$. On the basis of experimental data concerning carbamate and thiocarbamate compounds, the substitution of an oxygen atom by sulfur gives rise to a difference of about 1.5 eV (12 000 cm$^{-1}$) for the first $\pi \rightarrow \pi^*$ transition.[44]

Based on these considerations we conclude that the shoulder at $\sim$34 000 cm$^{-1}$ is due to c.t. transition involving a $S^{2-}$ ion localized at an edge or a step site (46 000 – 12 000 = 34 000 cm$^{-1}$). The shoulder at $\sim$40 000–41 000 cm$^{-1}$, in contrast, should arise from a peak that in pure MgO occurs at $\sim$53 000 cm$^{-1}$; this peak is due to c.t. excitations at the (100) terraces (53 000 – 12 000 = 41 000 cm$^{-1}$). Therefore, while adsorption of $CS_2$ is occurring prevalently on the edge sites, after desorption at 673–773 K, also a small fraction of sites on the (100) facelets and terraces must be involved. This demonstrates that at $T \cong$ 673–773 K some surface mobility is present. From our optical data, very little can be said about the corner sites, which are present in very small proportion. However, they are certainly involved in the oxygen–sulfur exchange.

At this point it becomes relevant to discuss which type of reactivity could have a S-doped MgO surface as compared with a pure MgO surface towards some probe molecules.

### 3.4 Interaction of CO with S-doped MgO samples

After changing the surface properties of MgO samples by a S-doping reaction, we have studied the reactivity of such S-doped MgO towards CO.

This is shown in Fig. 6, where the IR spectra of increasing doses of CO adsorbed at 100 K on the S-doped surface are reported. From these spectra, it appears immediately that negatively charged $(C_nO_{n+1})^{2-}$ species, due to the interaction of CO with unsaturated $O_{4c,3c}^{2-}$ ions, are completely absent. The only remaining band (very intense) at 2160–2150 cm$^{-1}$ is that previously associated with CO molecules adsorbed on the $Mg^{2+}$ ions of the surface. This allows us to conclude that the chemistry of the basic $O_{3c}^{2-}$ and $O_{4c}^{2-}$ ions is totally suppressed because these sites are involved preferentially in $O^{2-}$–$S^{2-}$ substitution. On the other hand, the data of Fig. 6 do not allow us to obtain definitive conclusions about the presence of $S^{2-}$ ions on the (100) facelets and terraces.

## 4. Bonding and energetics

In the previous section we have analyzed in detail the spectroscopic consequences of the reaction of the MgO surface with $CS_2$ and of the decoration of the low-coordinated sites with S atoms. In this section we consider the problem from a quantum chemical point of view. To this end the reaction mechanism of $CS_2$ with various O sites has been considered.

Model studies on the $Mg^{2+}$–$CS_2$ and $Mg^{+}$–$CS_2$ molecules show that these are bound complexes and that the bond is of an electrostatic nature. In the preferred adsorption mode the

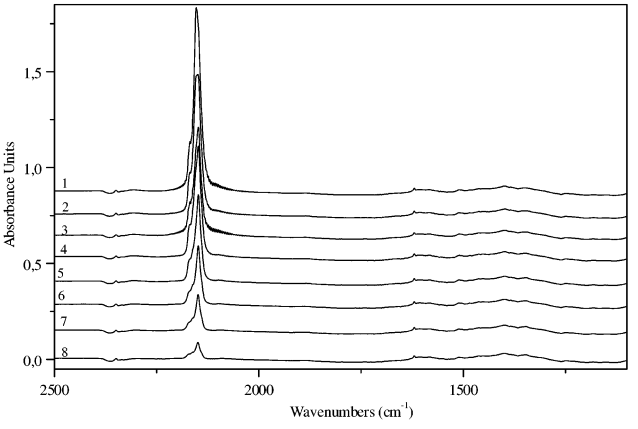


**Fig. 6** FTIR spectra of CO adsorbed at 100 K on S-doped MgO at decreasing coverages: from $p_{CO} = 5.32$ kPa (spectrum 1) to $p_{CO} = 0.133$ Pa (spectrum 8).

$CS_2$ molecule is linearly bound to the cation; the bond arises largely from the $CS_2$ polarization. The $D_e$ is 2.50 eV for $Mg^{2+}$–$CS_2$ and 0.10 eV for $Mg^{+}$–$CS_2$. The weak bonding in $Mg^{+}$–$CS_2$ reflects the low polarizability of $CS_2$. Any attempt to study physisorbed $CS_2$ on MgO results in unbound states even when $CS_2$ is interacting with exposed cations of the surface ($Mg_{4c}^{2+}$ and $Mg_{3c}^{2+}$ ions). This is different from the case of $CO_2$ which interacts with the surface cations of MgO to form weakly bound surface complexes.[10,11] This result is partly due to the inadequacy of the DFT approach to describe dispersive forces.

As discussed in the previous paragraphs the reaction of MgO anion sites with $CS_2$ leads to the formation of S-doped MgO, MgO(S),

$$MgO + CS_2 \rightarrow MgO(S) + COS \quad (11)$$

with a S atom replacing a lattice oxygen. The process implies a high energetic cost to remove the O atom, which is partially compensated for by the gain of incorporating a S atom. We have computed the cost of removing an O or a S neutral atom from the lattice. In both cases what is formed on the surface is an anion vacancy or F center, $F_s$, (the subscript s indicates the location of the vacancy on the surface). The results show that O is more strongly bound at a terrace site, 9.2 eV, than at a low-coordinated site, 7.8 eV, in agreement with previous calculations;[49,50] the bonding of a S atom at these sites is always smaller than for an O atom. The S atom is larger and induces a stronger local relaxation around it, Fig. 7. The Mg–S distances are $\approx$2.5 Å, more than 20% larger than the Mg–O distances. Because of its large size, the removal of a S atom from various sites costs about the same energy, $\approx$7 eV, Table 1. The effect of the higher Madelung potential at the terrace site, which stabilizes the anion, is compensated by the larger strain induced by the five-coordinated S atom. In all cases, if one considers as a reference the atomic states and the MgO surface with an anion vacancy, the substitution of an O atom with a S atom is endothermic, Table 1.

In contrast, if reaction (11) is considered, with formation of a COS molecule, the sulfur incorporation process is exothermic, independently of the site where the $CS_2$ molecule interacts, Table 2. This is because the formation of a C=O bond at the expense of a C=S bond overcompensates for the energy required to extract an O atom from the surface and to replace it with a S atom. Consistent with the trend in incorporation energy, the low-coordinated sites, edges, steps and corners, are much more reactive. In fact, while on a terrace site the process is exothermic by 0.27 eV only, on the low-coordinated sites the energy gain is 1.5 eV or more, see $\Delta E$ in Table 2.

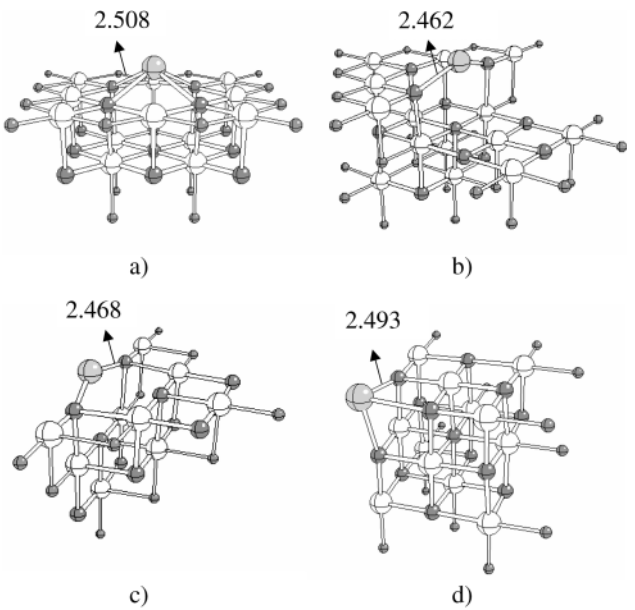


**Fig. 7** Same clusters as in Fig. 3, but with a S atom replacing the active O atom. Distances (in Å) between the S atom and the Mg nearest neighbors are shown. White spheres: O atoms; light gray spheres: S atom; dark gray spheres: Mg atoms; small gray spheres: ECPs.

**Table 1** Formation energies, $E_F$, of an oxygen vacancy, $F_S(O)$, or of a sulfur vacancy, $F_S(S)$, on the surface of MgO or S-doped MgO

| | $E_F$/eV | |
|---|---|---|
| Site | $F_S(O)$ | $F_S(S)$ |
| Terrace | 9.20 | 7.00 |
| Step | 8.10 | 7.08 |
| Edge | 7.98 | 7.24 |
| Corner | 7.77 | 6.79 |

**Table 2** Dissociation energy, $D_e$, of $CS_2$ bound on the MgO anion sites, energy change, $\Delta E$, and activation energy, $\Delta E^{\neq}$, of the reaction $MgO + CS_2 \rightarrow MgO(S) + COS$. Values in eV

| Site | Structure[a] | $D_e$[b] | $\Delta E$[c] | $\Delta E^{\neq}$[d] |
|---|---|---|---|---|
| Terrace | A | 0.44 | −0.27 | 3.40 |
| Step | B | 2.33 | −1.45 | 2.19 |
| Edge | C | 2.03 | −1.74 | 2.27 |
| | D | 0.76 | | |
| Corner | E | 1.18 | −1.49 | 1.22 |

[a] See Fig. 8. [b] $D_e$ for the reaction $MgO–CS_2 \rightarrow MgO + CS_2$ corrected for the BSSE. Positive values correspond to bound complexes. [c] A negative $\Delta E$ corresponds to an exothermic process. [d] See Fig. 10 for the structure of the transition state at an edge site; the other transition states have a similar structure.

The first step in the reaction is the formation of a MgO–$CS_2$ surface complex. $CS_2$ interacts with the $O^{2-}$ anions of MgO with formation of a surface thiocarbonate, $[OCS_2]^{2-}$, Fig. 8. In all cases, the resulting MgO–$CS_2$ complex is bound with respect to MgO and free $CS_2$. After correction for the BSSE, on a terrace site the binding is 0.44 eV, while on an edge or step site the binding is greater than 2.0 eV, Table 2. On low coordinated sites, the process is non-activated, as has been found for $CO_2$ on MgO,[10,11] while on a terrace site we have found a very small barrier. The reasons for the different behavior of high- and low-coordinated O sites have been analyzed in detail in ref. 11. At low-coordinated sites the Madelung potential of the ionic surface is lower and the $O^{2-}$ ion is less stabilized than at regular terraces or in the bulk. This results in a more pronounced tendency to transfer charge to an adsorbed molecule. In other words, the low-coordinated anions are more basic than the corresponding fully coordinated anionic centers.[11]

The interaction energy of $CS_2$ with MgO, $E_{tot}(z)$, was studied as a function of its distance from the surface by dividing it into two additive contributions:[11]

$$E_{tot}(z) = E_{act}(z) + E_{int}(z) \quad (12)$$

$E_{act}(z)$, where $z$ is the O–$CS_2$ distance, is the cost to bend the molecule, and to activate it. As $z$ decreases the SCS angle is reduced and the C–S bond elongated, with a destabilization of the molecule. $E_{act}(z)$ is obtained by computing the energy of the $CS_2$ molecule with the same geometry that it assumes when it is adsorbed at a given distance $z$ from the surface. The second term, $E_{int}(z)$, is the energy gain arising from the interaction of the "activated" $CS_2$ molecule with the surface. This term is attractive and may or may not compensate for the cost of activation. The two terms were estimated by computing the

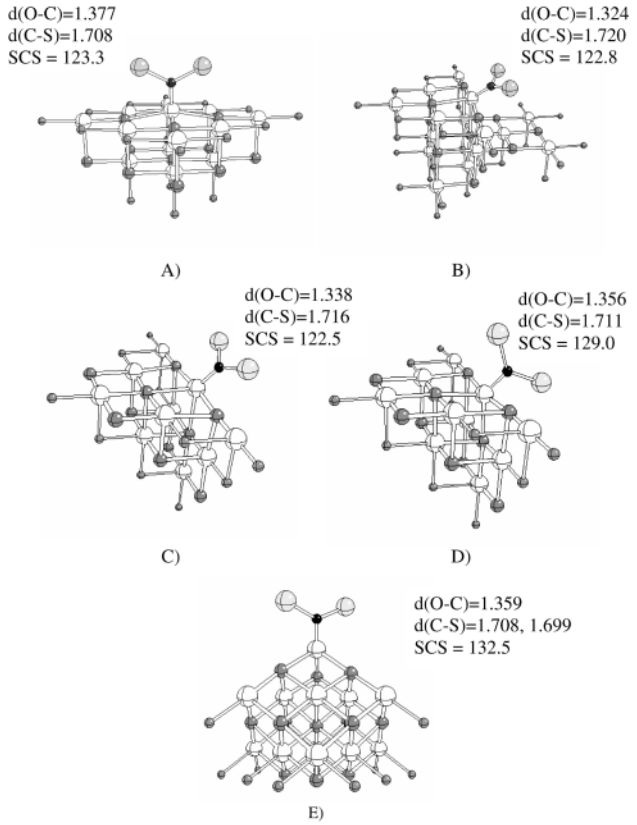


**Fig. 8** Optimized structures of the complexes [MgO–$CS_2$] formed after adsorption of $CS_2$ on different O sites of the MgO surface. (A) terrace, (B) step, (C) edge parallel, (D) edge perpendicular, (E) corner. Significant bond lengths (Å) and bond angles (°) are reported. The computed $d$(C–S) in gas phase $CS_2$ is 1.562 Å (theory). Black sphere: C atom; remaining spheres: as in Fig. 7.

potential energy curve for the interaction of $CS_2$ with a small $OMg_5$ cluster embedded in ECPs and PCs at various $z(O_{5c}$–$CS_2)$ distances; for each $z$ value, the C–S bond length and the SCS angle were optimized. The three curves, $E_{tot}(z)$, $E_{act}(z)$, and $E_{int}(z)$, are shown in Fig. 9. Clearly the first term, $E_{act}(z)$, is purely repulsive (and is defined negative) while the second term is attractive at least when the surface–$CS_2$ distance is not too short. At very short distances also the interaction between the promoted molecule and the surface is dominated by the Pauli

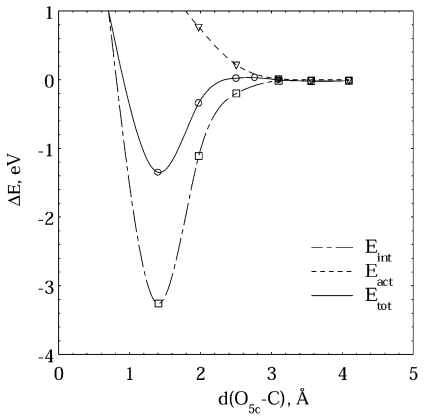


**Fig. 9** DFT-B3LYP potential energy curves for the interaction of $CS_2$ with the five-coordinated oxygen atom of the MgO (100) surface. The interaction energy curve, $E_{tot}$, is decomposed into the sum of the energy required to activate the $CS_2$ molecule, $E_{act}$, and the binding energy between the activated $CS_2$ molecule and the surface, $E_{int}$ (see text).

repulsion. The cost to bend and stretch the $CS_2$ molecule as in the MgO/$CS_2$ complex for $z \approx z_e$ is about 1.9 eV. The energy gain for the interaction of activated $CS_2$ with the cluster is about 3.2 eV and the net result is a bonding of about 1.3 eV (with the bigger cluster $[O_{13}Mg_{13}]+16$ ECPs the binding energy before the BSSE was 0.9 eV). Thus, the interaction is the result of two large but canceling contributions. Also the existence of a small barrier becomes clear from the analysis of the curves shown in Fig. 9. At $z(O_{5c}$–$CS_2) \approx 2.8$ Å a very small barrier of 0.03 eV is found. At this distance $CS_2$ begins to bend significantly (the SCS angle becomes 165°) but the price for the activation is not entirely compensated by the gain in formation of the surface thiocarbonate; as $z$ decreases, the $E_{int}(z)$ term dominates and the curve becomes attractive.

On all the surface complexes, terrace, edge, step, and corner, the $CS_2$ molecule is substantially activated and distorted, Fig. 8; the C–S bond is elongated from 1.562 Å (gas-phase) to 1.720 Å when the adsorption occurs at a step site, while the SCS angle goes from 180° in the gas-phase to 120–130° on the surface. The distortion of the adsorbed $CS_2$ molecule is a direct consequence of the charge transfer from the surface. While the adsorption energy varies considerably from site to site, Table 2, the geometry of chemisorbed $CS_2$ is similar, Fig. 8.

The mechanism for incorporation of a S atom at the expenses of a surface O atom was investigated by performing a search of the transition state for reaction (11). The barriers for the reaction and the geometry of the transition states were also determined, see Fig. 10 for an edge site and Table 2. The other transition states have a similar structure and are not reported. The barrier is largest for a terrace site, 3.4 eV, and lowest for a corner site, 1.22 eV; $O_{4c}^{2-}$ anions are replaced with barriers of 2.27 eV, Table 2 and Fig. 10. This is consistent with the fact that a lower coordination of the anion favors the incorporation of the bulky S atom. This result suggests that the sites that will react first will be the most reactive $O_{3c}^{2-}$ anions, followed by those at steps and edges, $O_{4c}^{2-}$, and that only at elevated temperatures is the reaction of the $O_{5c}^{2-}$ terrace sites expected. As soon as the S atom enters the MgO lattice, the corre-

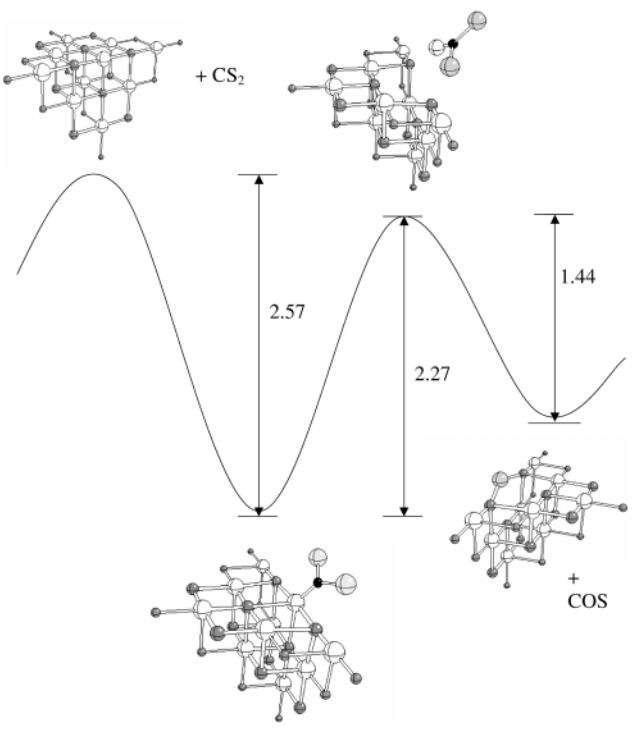


**Fig. 10** Energy profile for the reaction between $CS_2$ and a $O_{4c}^{2-}$ ion at an edge site of the MgO surface. All the structures correspond to stationary points on the potential energy surface. Energy values are in eV.

**Table 3** Computed harmonic stretching frequencies, $\omega_o$, and frequency shifts, $\Delta\omega$, for $CS_2$ adsorbed on various O sites of the MgO surface. All values are in $cm^{-1}$. Intensities, in parentheses, are in km $mol^{-1}$

| Site | $\omega_o$(O–C) | $\omega_o$(C–S)[a] | $\Delta\omega$(C–S)[b] |
|---|---|---|---|
| Terrace, $O_{5c}$ | 1074 (372) | 1048 (439) | −509 |
| Step, $O_{4c}$ | 1260 (417) | 1038 (421) | −519 |
| Edge, $O_{4c}$ | 1205 (468) | 1046 (423) | −511 |
| Corner, $O_{3c}$ | 1159 (361) | 1065 (526) | −492 |
| Exp. | | ≈1025–1105 | ≈ −420 to −500 |

[a] Gas phase $CS_2$: theory 1557 $cm^{-1}$, experiment 1533 $cm^{-1}$. [b] $\Delta\omega$ is computed with respect to the gas phase value.

sponding COS molecule desorbs from the surface without leading to an adsorbed complex. Thus, COS does not chemisorb on S sites of S-doped MgO. Hence the kinetics of the reaction is limited by the incorporation step, and does not imply the formation of other intermediates.

The strong distortion induced by the interaction with the surface results in pronounced shifts in the vibrational frequencies (see Section 3). These were determined by a full vibrational analysis and compared with the experimental IR spectrum, Fig. 4 and Table 3. According to the DFT calculations, the surface $[OCS_2]^{2-}$ complex results in C–S stretching modes at 1040–1060 $cm^{-1}$, red-shifted by about 500 $cm^{-1}$ with respect to the gas-phase molecule. This is in agreement with the experimental results which show a broad band at 1025–1125 $cm^{-1}$. We notice that no significant difference is found in the stretching properties of $CS_2$ adsorbed on various MgO sites, Table 3. In this respect, vibrational spectroscopy is probably not sufficient to detect the various sites where the thiocarbonate forms. On the other hand we have shown that UV–visible measurements are useful for a more precise identification of the sites responsible for the $CS_2$ adsorption.

Hence a comparison of the results obtained from IR and UV–visible measurements is essential to obtain more precise information concerning the active surface sites.

## 5. Conclusions

It has been demonstrated that when MgO surfaces are doped with $S^{2-}$ anions, which replace $O^{2-}$ anions located on steps and edges, the surface properties are drastically modified.

S-doped MgO samples are produced by interaction of carbon disulfide, $CS_2$, with polycrystalline MgO through exchange reactions, causing the formation of $Mg^{2+}$–$S^{2-}$ clusters in the MgO matrix. The analysis of the IR and UV–visible spectra shows the formation of COS and even $CO_2$ species, indicating the incorporation of S atoms at the MgO surface. The reaction proceeds through the formation of surface complexes of the type $[OCS_2]^{2-}$ followed by successive elimination of COS. The reaction is exothermic as shown by first principle calculations because the formation of a C=O bond at the expense of a C=S bond in the product overcompensates for the energy required to replace an O atom with a S atom on the surface. The spectral evidence also shows that at low temperature the reaction occurs at low-coordinated O anions, mostly at steps and edges, while the terrace five-coordinated O anions are unreactive under normal conditions. This is consistent with the higher exothermicity and lower energy barriers associated with the reaction occurring at low-coordinated anions.

The presence of the S atoms at the surface of MgO completely changes the reactivity of the oxide, and transforms the reactive polycrystalline material into a chemically inert system.

The reactivity towards CO of pure and S-doped MgO surfaces is completely different, as shown by comparing Fig. 1 (CO adsorbed on pure MgO sample) and Fig. 6 (CO adsorbed on a S-doped MgO sample). This is because all the step, edge and corner O anions have been replaced by inert S atoms, thus eliminating completely the original reactivity of $O_{3c}^{2-}$ and $O_{4c}^{2-}$ ions at the MgO surface, which by interaction with CO give rise to negatively charged $(C_nO_{n+1})^{2-}$ species. This modified reactivity of S-doped MgO samples as compared with the pure MgO samples has also been tested with other probe molecules (data not reported for sake of brevity).

## Acknowledgements

Financial support from the Ministry of University and Research (MURST) through the National Program: "Strati ultrasottili di ossidi e solfuri inorganici: crescita, caratterizzazione e reattività superficiale" is gratefully acknowledged. The work of one of us (G. P.) is also supported through the PRA–ISADORA project of the Istituto Nazionale per la Fisica della Materia.

## References

1 G. Pacchioni, *Surf. Rev. Lett.*, 2000, **7**, 277.
2 G. Pacchioni, in *The Chemical Physics of Solid Surfaces—Oxide Surfaces*, ed. P. D. Woodruff, Elsevier, Amsterdam, 2001, vol. 9, p. 94.
3 E. Escalona Platero, D. Scarano, G. Spoto and A. Zecchina, *Faraday Discuss. Chem. Soc.*, 1985, **80**, 183.
4 E. Escalona Platero, D. Scarano, A. Zecchina, G. Meneghini and R. De Franceschi, *Surf. Sci.*, 1996, **350**, 113.
5 D. Scarano, G. Ricchiardi, S. Bordiga, P. Galletto, C. Lamberti, G. Spoto and A. Zecchina, *Faraday Discuss.*, 1996, **105**, 119.
6 H. J. Freund, H. K. Kuhlenbeck and V. Staemmler, *Rep. Prog. Phys.*, 1996, **59**, 283.
7 R. Soave and G. Pacchioni, *Chem. Phys. Lett.*, 2000, **320**, 345.
8 A. Zecchina, S. Coluccia, G. Spoto, D. Scarano and L. Marchese, *J. Chem. Soc., Faraday Trans.*, 1990, **86**, 703.
9 A. Zecchina and F. Stone, *J. Chem. Soc., Faraday Trans. I*, 1978, **74**, 2278.
10 G. Pacchioni, *Surf. Sci.*, 1993, **281**, 207.
11 G. Pacchioni, J. M. Ricart and F. Illas, *J. Am. Chem. Soc.*, 1994, **116**, 10 152.
12 L. Marchese, S. Coluccia, G. Martra, E. Giamello and A. Zecchina, *Mater. Chem. Phys.*, 1991, **29**, 437.
13 E. Giamello, D. Murphy, L. Marchese, G. Martra and A. Zecchina, *J. Chem. Soc., Faraday Trans.*, 1993, **89**, 3715.
14 D. Scarano, G. Spoto, S. Bordiga, S. Coluccia and A. Zecchina, *J. Chem. Soc., Faraday Trans.*, 1992, **88**, 291.
15 A. Zecchina, D. Scarano, S. Bordiga, G. Ricchiardi, G. Spoto and F. Geobaldo, *Catal. Today*, 1996, **27**, 403.
16 S. Coluccia, M. Baricco, L. Marchese, G. Martra and A. Zecchina, *Spectrochim. Acta, Part A*, 1993, **49**, 1289.
17 R. Wichtendahl, M. Rodriguez-Rodrigo, U. Härtel, H. Kuhlenbeck and H. J. Freund, *Phys. Status Solidii A*, 1999, **173**, 93.
18 (*a*) D. Sellmann and J. Sutter, *Acc. Chem. Res.*, 1997, **30**, 460; (*b*) R. H. Holm, P. Kennepohl and E. I. Solomon, *Chem. Rev.*, 1996, **96**, 2239.
19 J. A. Rodriguez and J. Hrbek, *Acc. Chem. Res.*, 1999, **32**, 719.
20 *Cluster Models for Surface and Bulk Phenomena*, ed. G. Pacchioni, P. S. Bagus and F. Parmigiani, NATO ASI Series B, Plenum, New York, 1992, vol. **283**, .
21 J. Sauer, P. Ugliengo, E. Garrone and V. R. Saunders, *Chem. Rev.*, 1994, **94**, 2095.
22 G. Pacchioni, A. M. Ferrari, A. M. Marquez and F. Illas, *J. Comput. Chem.*, 1997, **18**, 617.
23 N. W. Winter and R. M. Pitzer, *J. Chem. Phys.*, 1988, **89**, 446.
24 M. A. Nygren, L. G. M. Pettersson, Z. Barandiaran and L. Seijo, *J. Chem. Phys.*, 1994, **100**, 2010.
25 I. V. Yudanov, V. A. Nasluzov, K. M. Neyman and N. Rösch, *Int. J. Quantum Chem.*, 1997, **65**, 975.

26 *Chemisorption and Reactivity on Supported Clusters and Thin Films*, ed. R. M. Lambert and G. Pacchioni, NATO ASI Series E, Kluwer, Dordrecht, 1997, vol. 331.
27 K. M. Neyman, G. Pacchioni and N. Rösch, in *Recent Development and Applications of Modern Density Functional Theory, Theoretical and Computational Chemistry*, ed. J. Seminario, Elsevier, Amsterdam, 1996, vol. 4, p. 569.
28 A. D. Becke, *J. Chem. Phys.*, 1993, **98**, 5648.
29 C. Lee, W. Yang and R. G. Parr, *Phys. Rev. B*, 1988, **37**, 785.
30 R. Ditchfield, W. J. Hehre and J. A. Pople, *J. Chem. Phys.*, 1971, **54**, 724.
31 W. J. Hehre, R. Ditchfield and J. A. Pople, *J. Chem. Phys.*, 1972, **56**, 2257.
32 S. F. Boys and F. Bernardi, *Mol. Phys.*, 1970, **19**, 553.
33 H.B. Schlegel, *J. Comput. Chem.*, 1982, **3**, 214.
34 C. Peng, P. Y. Ayala, H. B. Schlegel and M. J. Frish, *J. Comput. Chem.*, 1996, **17**, 49.
35 K. Nakamoto, *Infrared Spectra of Inorganic and Coordination Compounds*, Wiley-Interscience, New York, 3rd edn., 1977.
36 A. Sahibed-Dine, A. Aboulayt, M. Bensitel, A. B. Mohammed Saad, M. Daturi and J. C. Lavalley, *J. Mol. Catal. A*, 2000, **162**, 125.
37 A. Zecchina, M. G. Lofthouse and F. S. Stone, *J. Chem. Soc., Faraday Trans I*, 1975, **71**, 1476.
38 S. H. R. Brienne, M. M. V. Bozkurt, S. R. Rao, Z. Xu, I. S. Butler and J. A. Finch, *Appl. Spectrosc.*, 1996, **50**, 521.
39 L. H. Little, *Infrared Spectra of Adsorbed Species*, Academic Press, London and New York, 1966.
40 S. J. David and B. S. Ault, *J. Phys.Chem.*, 1982, **86**, 4618.
41 S. J. David and B. S. Ault, *Inorg. Chem.*, 1985, **24**, 1048.
42 C. N. R. Rao, *Ultra-Violet and Visible Spectroscopy*, Butterworth, London, 1975.
43 A. Muller, N. Mohar, P. Cristophliemk, I. Tossidis and M. Drager, *Spectrochim. Acta, Part A*, 1973, **29**, 1345.
44 Y. Ozias and L. Reynard, *Theoret. Chim. Acta*, 1971, **20**, 51.
45 C. K. Jörgensen, in *Progress in Inorganic Chemistry*, ed. S. J. Lippard, Interscience, New York, 1970, vol. 12, p. z101.
46 A. Zecchina and F. Stone, *J. Chem. Soc., Faraday Trans. I*, 1976, **72**, 2364.
47 E. Garrone, A. Zecchina and F. S. Stone, *Philos. Mag. B*, 1980, **42**, 683.
48 P. V. Sushko, A. L. Shluger and C. R. A. Catlow, *Surf. Sci.*, 2000, **450**, 153.
49 L. N. Kantorovich, J. M. Holender and M. J. Gillan, *Surf. Sci.*, 1995, **343**, 221.
50 G. Pacchioni and P. Pescarmona, *Surf. Sci.*, 1998, **412/413**, 657.